Grid effects on tsunamis in nearshore regions

Geir Pedersen

March 15, 1995

Abstract

We investigate the limitations of long wave models for tsunami propagation through two idealized cases. The reproduction of amplification of normally incident waves is studied by simulation of plane waves with hydrostatic and Boussinesq models. Special emphasize is put on the validity of Greens law and implications for run-up calculations. In the other case a staircase boundary representation of a curved coastline is tested. It turns out that spurious effects easily become dominant in the nearshore domain, even in simple geometries.

1 Introduction

There are several techniques available for solving partial differential equations in geometries with curved boundaries. The most powerful alternative is probably the finite element technique, while comparatively simple geometries, at least, can be treated effectively through invocation of curvilinear grids. However, for linear shallow water equations the straightforward method of replacing the true boundary by a "staircase" boundary is still extensively used. Even though this approach yields a rather crude first order representation of the coastline this is generally regarded as outweighed by the simple implementation and effectiveness of the resulting code.

At first glance a staircase boundary might be expected to create a large amount of noise and possibly a series of additional crucial spurious effects. However, experience shows that for quite a number of applications this is not the case. On the other hand, a closer scrutiny sometimes reveals that staircase boundaries may introduce qualitatively new features even in very simple contexts. We will refer a simple and relevant example. A vertical impermeable wall situated in deep water and aligned at an angle 45° to the grid axes, will reflect incident waves without creation of any appreciable noise. Still, as shown in [7] and [6] such a boundary may act as a guide for trapped waves even in constant depth.

In tsunami calculations we want to extend the calculations of our models as close to the shoreline as possible, even though the actual runup motion generally is achievable only through application of nonlinear fine scale models including a moving shoreline description. As a wave propagates in shoaling water its length will decrease. According to geometrical optics the wavelength will be proportional to $h^{\frac{1}{2}}$ (h - depth)

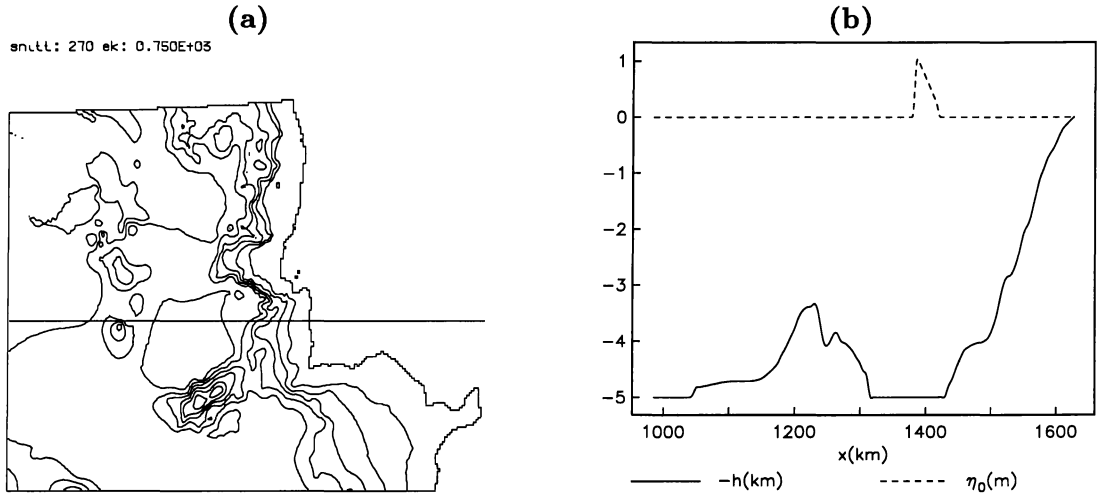

Figure 1: (a) Contour plot of the Iberian sea outside Portugal. The straight E-W line shows the cross-section defining the geometry for the 2D calculations. (b) Depth profile of cross-section and initial disturbance.

for waves of approximately normal incidence. On the other hand, any second order finite difference scheme for long waves will possess a dispersion relation of the form

$$c_n = c_a(1 + q_1 k^2 \Delta x^2 + q_2 \omega_a^2 \Delta t^2 + q_3 k \omega_a \Delta x \Delta t) + O(\Delta x^3, ...) \qquad (1)$$

where c_n and c_a are numerical and analytical wave speed respectively, ω_a the analytical frequency, k the wave number, Δx and Δt the grid increments, and q_1, q_2, q_3 are coefficient specific for the actual method. It is then readily deduced that the relative importance of numerical dispersion is proportional to h^{-1} for a fixed Δx[1]. In the limit $h \to 0$ results from geometrical optics become completely inappropriate and the wavelength, defined in some sense or another, approaches a finite value. Additional problems may, however, be anticipated due to the singularity at the shoreline point that may give rise to a logaritmic singularity in the surface elevation and a first order pole in the velocity. Still, it has been verified that even the simplest linear numerical schemes may provide good run up estimates in 2D calculations, as long as a noflux condition is properly applied at the shore [1]. When discussing 3D calculations we must consider the combined effects of staircase boundaries and the singularity and further difficulties may arise. In this report we intend to shed some light on these problems through some simple numerical experiments and observations.

[1] It is noteworthy that the importance of the Δt^2 term remains unaltered due to the invariance of the period.

2 Plane waves in shoaling water – a 2D test case.

We have generated a two dimensional geometry by extracting an E-W cross section roughly midway between Lisbon and Cabo de Sao Vincente, as shown in figure 1, from the depth matrix for the Iberian sea made available to us by P. Miranda from the Lisbon university in 1993. The figure also displays an initial surface elevation corresponding to an uplift zone of the sea bottom, running South-North, of width a=25km and maximum height Δh = 1m. The source is situated at a depth of 5000m, just outside the continental shelf. Both the geometry and the source inherit characteristic dimensions which we believe to be typical for the Iberian tsunami incidents. [2] We have performed computations using the linear hydrostatic equations and the Boussinesq equations, with and without the nonlinear terms. There are three main intentions behind these simulation: (i) estimate the nonlinear and dispersive effects, (ii) study the grid dependence in shallow regions, (iii) determine the amplification with special emphasize on the validity of Greens law that states that the amplitude is proportional to $h^{-\frac{1}{4}}$.

The Boussinesq equations, based on the depth averaged velocity, as well as the numerical technique are adopted from [4] and [8]. However, the results reported below is not likely to be very dependent on details in the solution procedure.

Applying spline interpolation to the original depth data, we have defined a twice differentiable bottom function that enables the construction of grids of arbitrary resolution and distribution of grid points. Computations have been carried out for grid increments ranging from Δx = 10km to Δx = 208m (5km/24). In a related study of wave propagation across a seamount as well as in runup calculations in an idealized geometry we have employed an optimal, nonuniform, distribution of grid points with very good results. However, while this technique may be applicable to 3D finite element methods it has no really practical extension to 3D finite difference simulations.

In addition to snapshots of the surface elevation and time series the solutions are investigated through the secondary unknowns $\eta_{\max}$ and the extrapolated run-up .The quantity $\eta_{\max}$ is the maximum surface elevation at any instant and may be displayed as function of time or the depth at which it occurs. We extrapolate the runup using the two neighbouring points to the shore and assuming a linear dependence of η and h upon the space coordinate. The values corresponding to $h = 0$ are then interpreted as the run-up height.[3]

2.1 Nonlinear and dispersive effects.

For weakly dispersive waves we have the dispersion relation $c = c_0(1 - \frac{1}{6}(kh)^2 + ...)$ where c_0 is the phase speed of infinitely long waves. Assuming again that the

[2] The simulation was originally designed as a first study of wave generation from a fault parallel to the Portuguese coast, but this is inessential in the present context.

[3] This extrapolation makes sense only if h is small in the vicinity of the shore.

wavelength is determined by geometrical optics we find that the relative importance of dispersion is proportional to h.

To demonstrate the effect of dispersion on disturbances of different shapes we have computed wave propagation from the three initial conditions in figure 2(a). In addition to the shape from figure 1 (marked "tilt" or "tiltslab") we have employed a smooth shape (marked bell) and finally a shape resembling the displacement fields obtained from Okadas formula [2] (marked Okada). After 8 minutes the waves are still in deep water and the effect of dispersion is noticeable for all shapes. In addition to the production of a residual wave train the dispersion effect reduces the height of the leading pulse by roughly 20-30% as shown in figure 2(c-d). The most distinguished difference between the sources concerns the trailing wave system. While the first trough is of the same order of magnitude the wavetrain from the smooth bell source, in contrast to the other options, displays only a few appreciable oscillations. For the Okada source, in particular, we also observe waves too short to be described properly by the Boussinesq equations. At this point it is an appropriate digression to discuss the wave generation mechanism briefly. In shallow water theory we generally assume an instantaneous surface elevation equal to the uplift of the bottom. However, if we had invoked a fully non-hydrostatic theory the bottom displacement could be replaced by a distribution of sinks and sources. Then, in view of the actual depth of 5000m we would then not generate gradients in the surface elevation as steep as in the Okada and "tilt" shapes. It would probably be more realistic to distribute the jumps corresponding to the fracture location over an distance of order one depth. To get a complete description of the energy transfer to water we should also take compression waves in the water into account.

Another point of some interest is the exponentially decaying "nose" of the dispersive solutions that may affect the time of first arrival. However, in this case the reduction of travel time hardly amounts to more than 10-15 seconds, say.

As demonstrated in figure 3(d) omission of dispersion terms also leads to overestimation of the extrapolated run-up. It is also noteworthy that while nonlinear effects are negligible in deep water their steepening effect is clearly visible in the run-up.

2.2 Discretization errors.

The plots of the surface elevation, 4(a-f), reveal that the linear hydrostatic solutions are subjected to a significant numerical dispersion in shallow water, even for the finest grid $\Delta x = 208$m. The result is a trailing noise that is very different from the effect of real dispersion, see for instance panel (a) or (c) in figure 4. As shown in figure 5(a-b) the discretization errors are small in deep water , but lead to serious underestimation in shallow water as demonstrated in figure 3 and 4. This is only partly due to the fact that the finer grids yield smaller depths near the shore. Even at $h = 19$m the tendency toward underestimation is clear for the coarser grids, see figure 5(b-c). The limitations for each resolution are probably demonstrated most clearly in the plots of $\eta_{\max}$ versus h in figure 6. For $\Delta x = 5$km the results start to deviate at a depth

of some hundred meters. The simulations with $\Delta x = 1.25$km becomes poor at a depth of some tenths of meters while the results from $\Delta x = 417$m and $\Delta x = 208$m separates only slightly even in the beach zone. We also note that the convergence is markedly better for the Boussinesq equations, even though no corrections to scheme are used.

2.3 Amplification – Greens law.

Denoting the depth in the source region by h_m (5000m) we display the dimensionless quantity $f = \eta_{\max}(h/h_m)^{\frac{1}{4}}/\Delta h$ as a function of h in figure 6. As long as Greens law ($\eta_{\max} \sim h^{-\frac{1}{4}}$) is fulfilled the depicted quantity then remains constant. For the linear hydrostatic solution, obtained from the finest grid, we observe a constant value of f close to one half down to about 5m. The value of one half is due to a nearly uniform splitting of the initial disturbance in one outgoing and one in-going wave. Correspondingly, the Boussinesq solution yields a constant f, slightly less than 0.4, that can be observed down to $h = 10$m, say. The reduction from 0.5 to 0.4 is due to dispersion during the early stages of the wave evolution in deep water, while the interval with a constant f indicates that dispersion effects are less important for h less than 1000m, say, since the water is shallower and the different wave components already have become separated.

The fact that coarse grids underpredict the amplification (decrease in f) may partly be explained by disintegration of the incident pulse due to numerical dispersion. However, also quantities like energy density and group velocity may be influenced by discretization errors and consequently combine to a different physical optics. These effects will investigated further in a subsequent report.

Finally we note that Greens law certainly overestimates the amplitude of the incident wave in the limit $h \to 0$, while the neglection of a reflected wave cause an underestimation concerning the total surface elevation. As a consequence we may observe a nearly constant f somewhat beyond the validity range of physical optics.

3 Geometry and set up for 3-D test.

We have chosen a simple set up for a simulation of the linear hydrostatic equations. The incident wave is a plane wave with a trigonometric hat shape that is specified in a region of constant depth. As an idealized model of the coastline we employ a symmetric bell shaped point adjoined at each side by a straight coastline. The bottom is sloping monotonously from the coast until the constant depth of the off shore region is attained. Since the the geometry as well as the incident wave are symmetric we perform calculations in half the domain only. In the present context it is convenient to employ a horizontal length scale, L, linked to the slope, while the constant depth, h_0, of the off shore region is used to make the surface elevation dimensionless. Accordingly the time scale becomes $L/\sqrt{gh_0}$. We may then express the incident wave through requiring zero velocity and imposing an initial surface

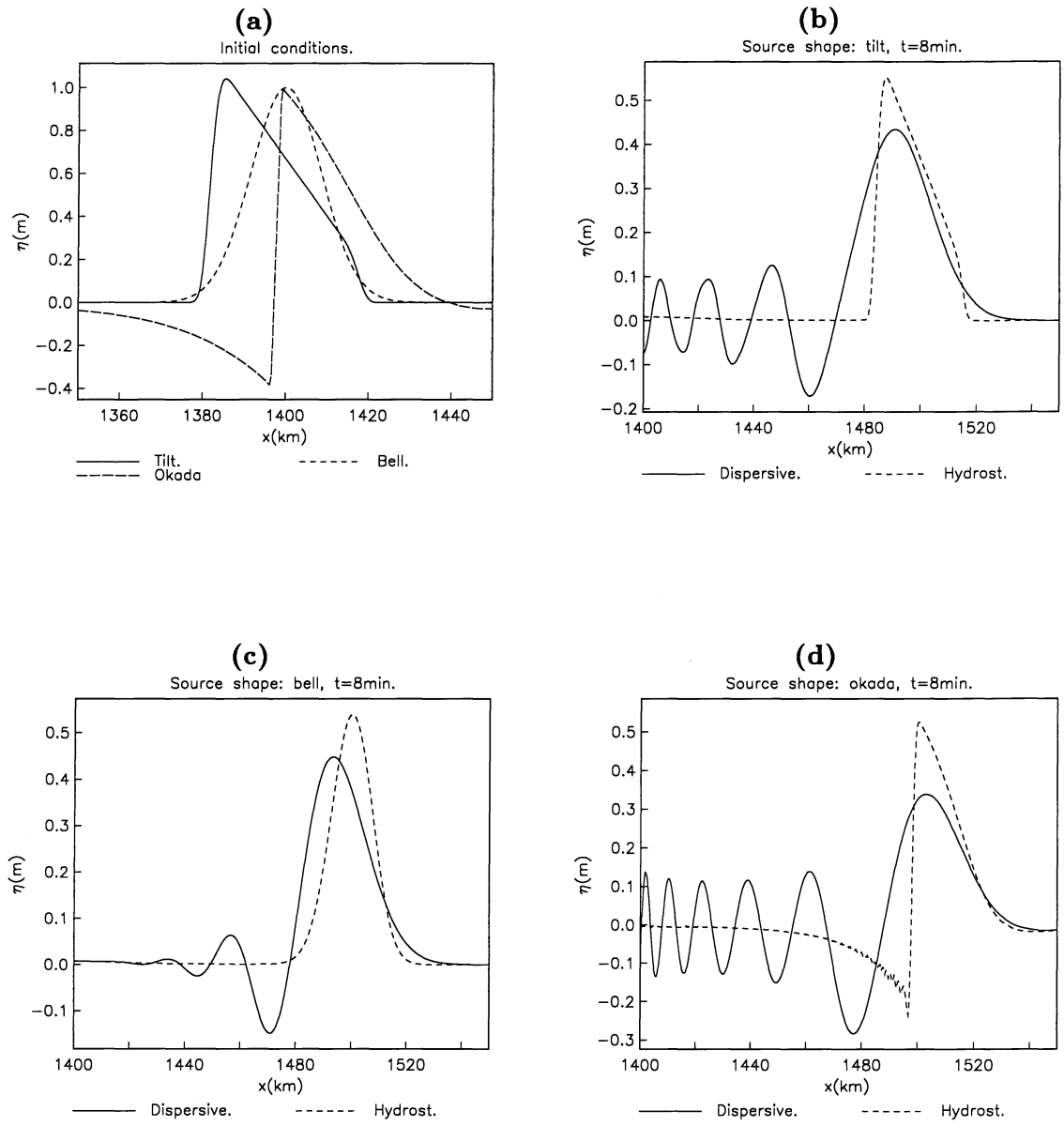

Figure 2: (a): The three different initial conditions. (b-d): The surface elevation at $t = 8$min. for the different source shapes as obtained by hydrostatic and dispersive theory. The grid increment is $\Delta x = 417$m.

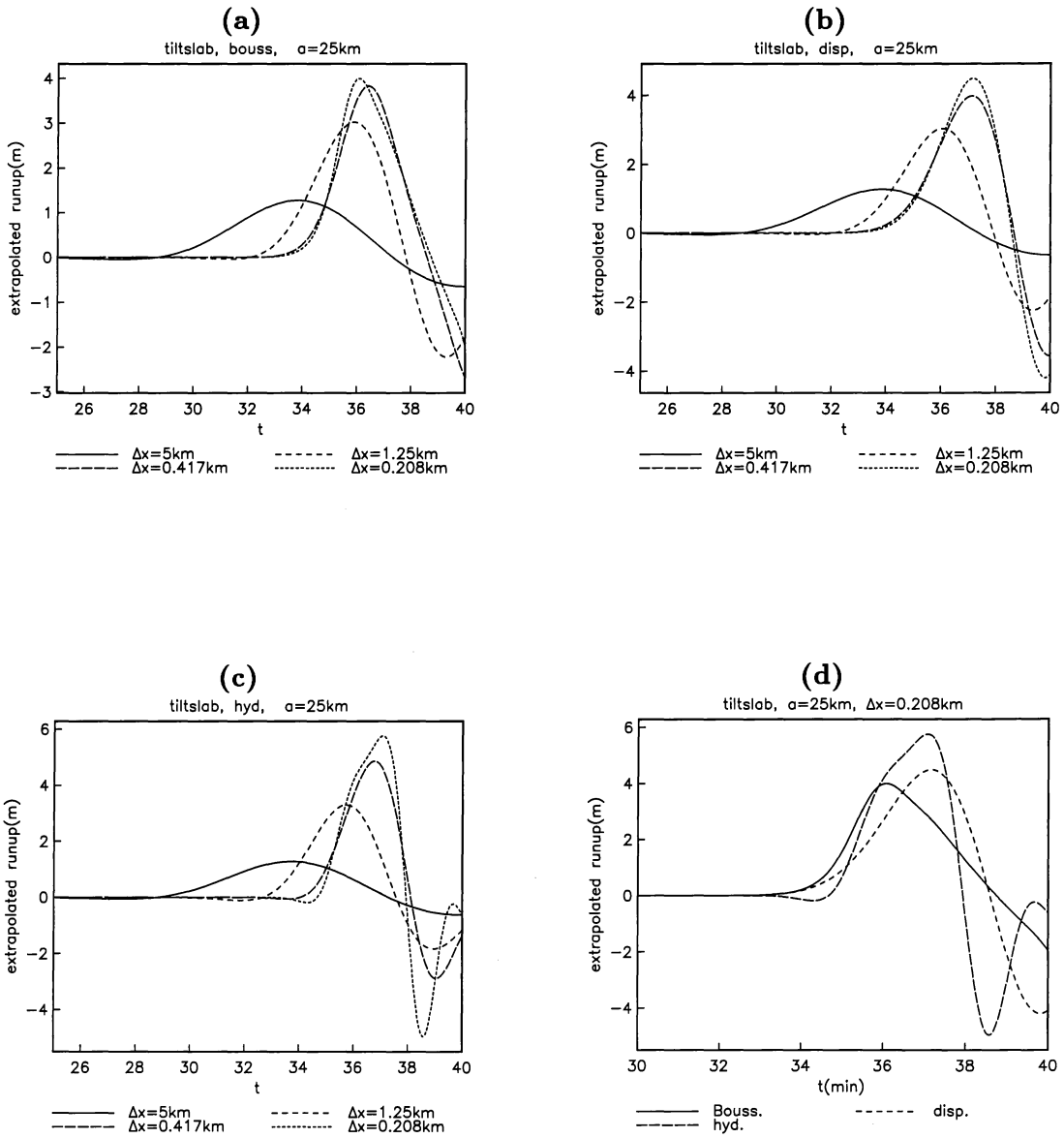

Figure 3: Extrapolated runup.

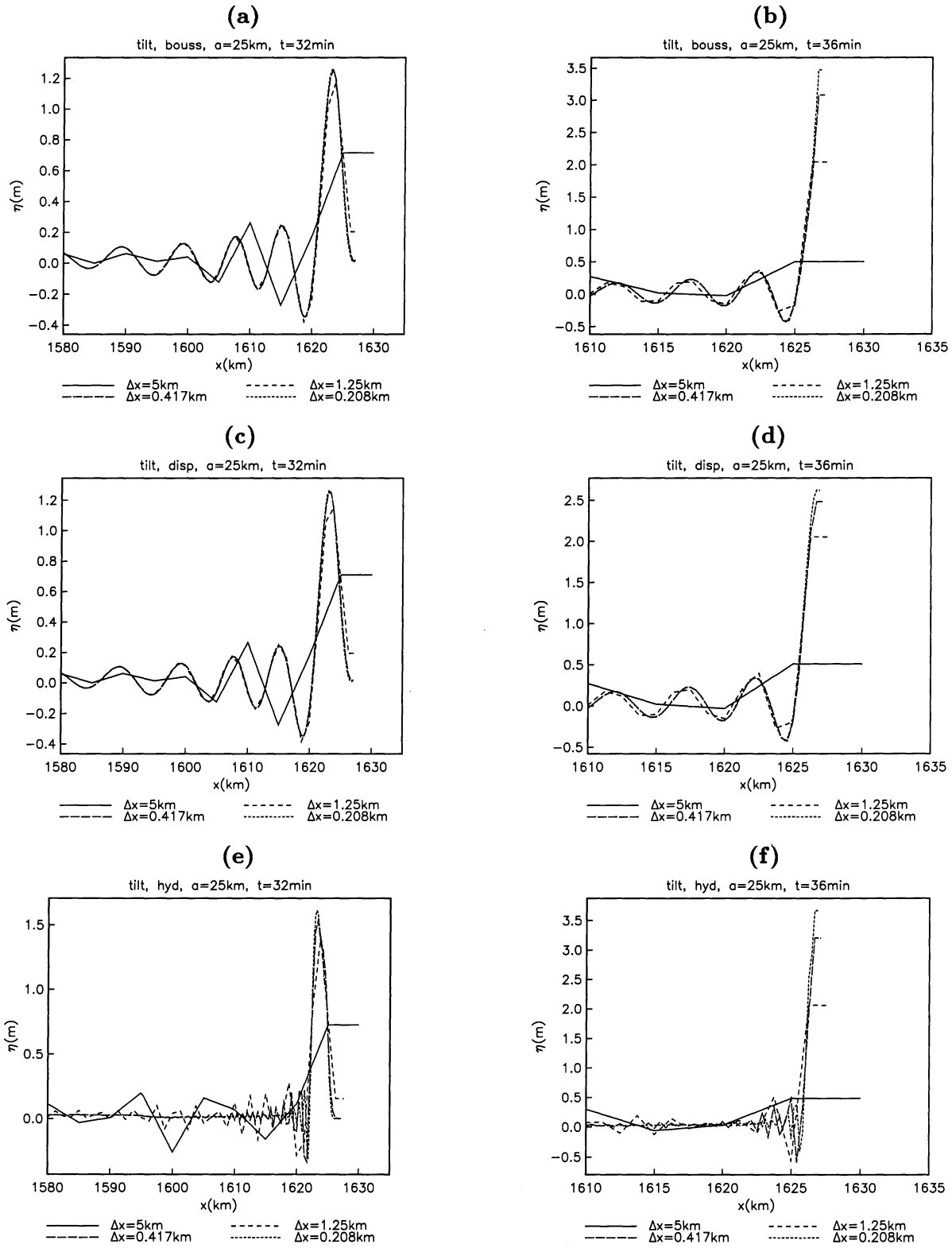

Figure 4: Surface elevation in shallow water.

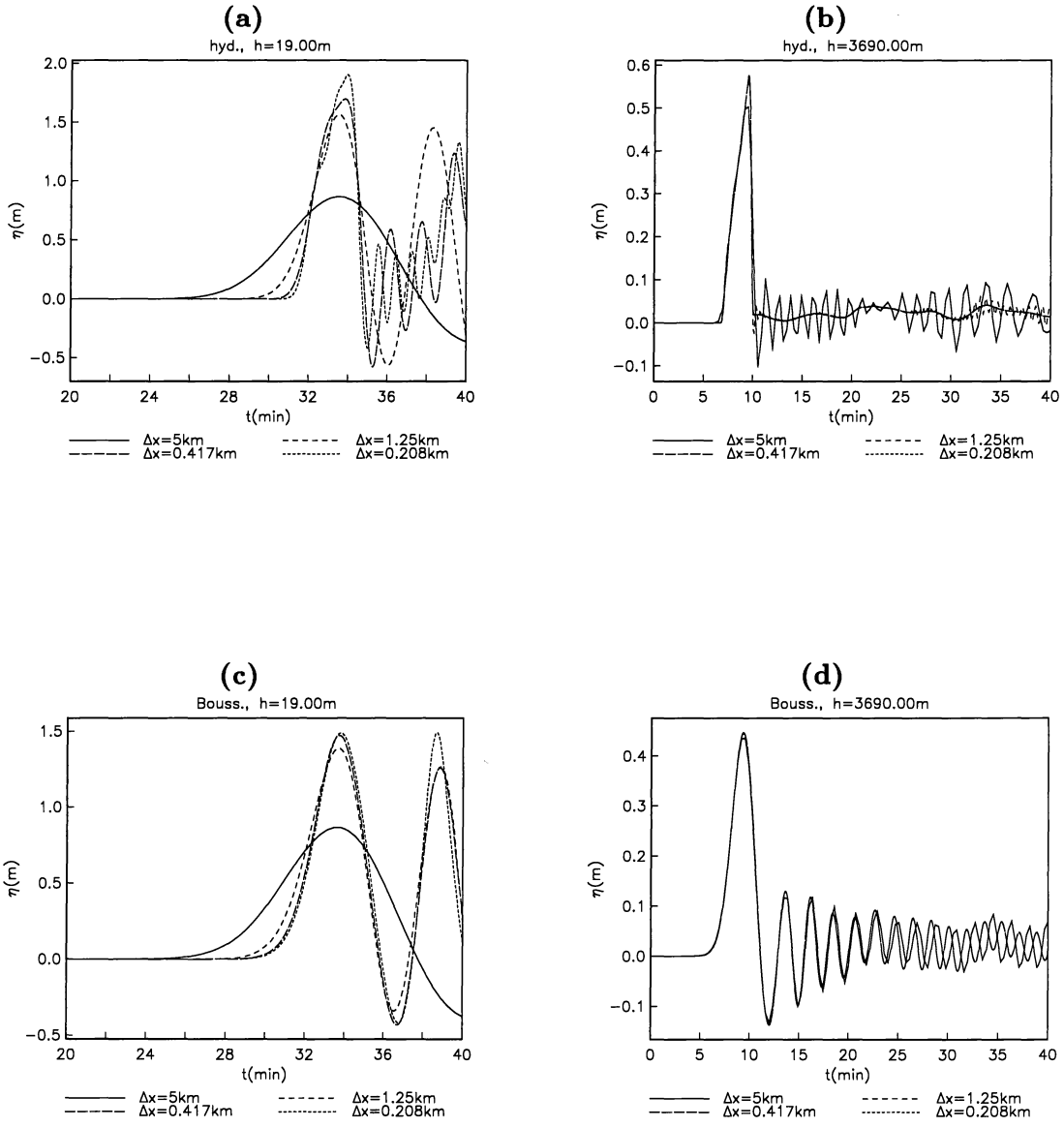

Figure 5: Time series of the surface elevation. (a-b): Hydrostatic linear equations, (c-d): Boussinesq equations

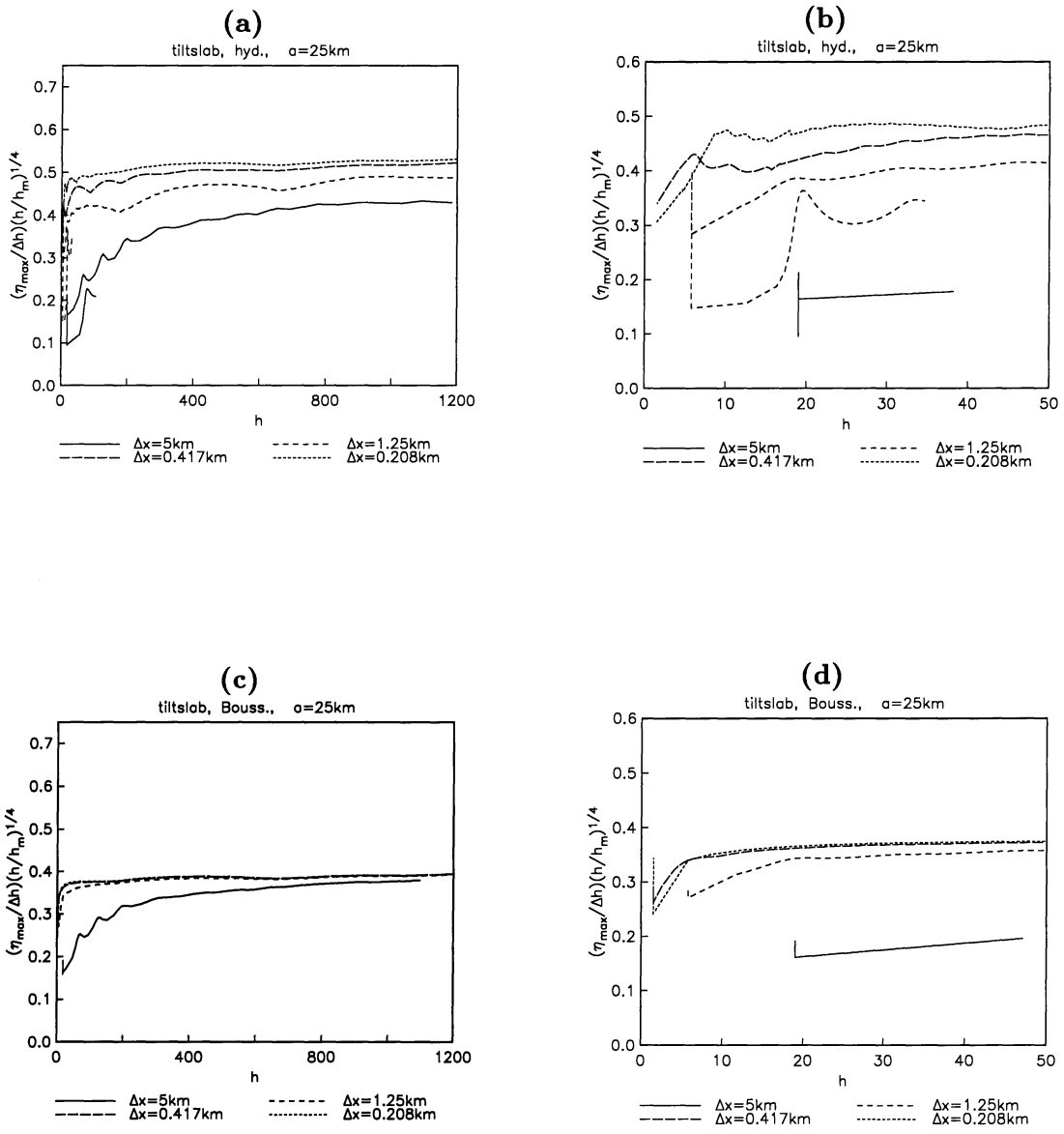

Figure 6: Amplification, Greens law. (a-b): Hydrostatic linear equations, (c-d): Boussinesq equations

elevation of the form:

$$\eta_{\text{in}} = A(1 + \cos(k(x - x_i))) \quad \text{for} \quad |k(x - x_i)| < \pi \tag{2}$$

where $k = 2\pi/\lambda$. In the linear approximation this initial condition leads to an incident wave of amplitude A.

The bottom topography is depicted in figure 7. A bottom profile at constant y contains a section of constant slope adjoined to a flat bottom section by a second order polynomial. At the upper y limit we introduce on half of a Gaussian shaped point implicitly completed by the application of a symmetry condition. The bottom function can be written:

$$h(x, y) = q(x - s(y)) \quad ; \quad s(y) = Be^{-(\frac{(y-y_p)}{r})^2} \tag{3}$$

where the depth profile is given by the continuously differentiable function.

$$q(\xi) = \begin{cases} \tan\theta\xi & \text{if} \quad \xi < \cot\theta - \ell \\ 1 - \frac{\tan\theta}{4\ell}(\xi - \cot\theta - \ell)^2 & \text{if} \quad -\ell < \xi - \cot\theta < \ell \\ 1 & \text{if} \quad \xi > \cot\theta + \ell \end{cases} \tag{4}$$

3.1 Choice of parameters

In the simulations reported below we have chosen L as to give $\tan\theta = \frac{1}{2}$, while the other parameters read: $A = 1$, $\lambda = 4$, $B = 3$, $r = 3$, $y_p = 80$ and $\ell = 0.25$. The total computational domain, $-1 < x < 47.241$, $39.9 < y < 80$, is large enough to prevent reflections from the lower and right boundaries to reach the vicinity of the peninsula. Simulations have been performed with 6 different resolutions. Employing the grid $\Delta x_1 = 0.241208$, $\Delta y_1 = 0.2005$ as a reference, we may write $\Delta x_\alpha = \alpha \Delta x_1$ etc. for $\alpha = 4, 2, 1, \frac{1}{2}, \frac{1}{4}, \frac{1}{8}$. We note that Δx_1 corresponds roughly to having the slope covered by 8 points, the incident wave resolved by 16 points and to have 15 points along half the curved part of the coastline.

4 Simulations

The incident wave is specified at a distance 10 from the straight part of the coastline and the equations are integrated over a time span of 75 dimensionless units. We have investigated the solutions by contour plots, time series and the surface elevation at the grid points adjacent to the shoreline. Naturally, the actual locations of these grid points depend on the resolution.

In a plane, linear run up calculation with the present incident wave and bottom slope we get a run up with maximum slightly above 3 followed by a back wash with a minimum of nearly -1.2, again followed by a smaller runup and gentle oscillations. The time series of the surface elevation at the free tip is depicted in figure 8. In the three dimensional setting we naturally experience a spatial variation, depending qualitatively on the parameters, of the run up at the headland. A topographic feature

as a point will also cause diffraction yielding waves radiated outward as well as edge waves trapped in the shore region.

In figure 9 through 11 we have shown contour plots of the surface elevation at selected times. The results obtained by the finer grids are depicted with the same resolution as $\alpha = 1$. At $t = 15$ we see the principal reflected wave moving outward. This wave is fairly well reproduced by even the coarsest grids and the results for the 2-3 finest grids are nearly identical. For the two coarsest grids, $\alpha = 4$ and $\alpha = 2$, we observe indications of short fluctuations at the point which we will return to in more detail below. At $t = 33$ we recognize a train of trapped waves moving in the negative y-direction. Finally, for $t = 42$, the edge wave production is still significant for the coarser grids while it has nearly vanished for the finest grid. The artificial prolongation of the generic period for edge waves is also seen in the time series of figure 12. It is quite clear that a effect of this type may corrupt the Fourier spectrum completely. As for the local behaviour of the shoreline at the point we refer to the results in figure 13. For $\Delta x = 0.2412$ ($\alpha = 1$) we observe strong fluctuation on the grid scale. However, this noise seems to be a forced response to the incident and reflected wave systems and a careful investigation do not reveal any sign of noticeable noise being transported either in the off shore direction or along the straight coastline.

Limiting the computations to $h \geq 0.15$ we obtain the results displayed in the figures 8(b), 12(c-d) and 16 through 17. We now observe a more rapid convergence with much less noise at the point and without the spurious continuation of edge wave emission from the point.

5 Concluding remarks

Numerical modeling in coastal waters will meet with at least three recognizable difficulties:

1. Wavelengths get shorter in the vicinity of the coastline thereby increasing the discretization errors.

2. Staircase boundaries will create noise in the coastal areas that for extreme cases may dominate the local solution. This noise will not spread to contaminate the solution at larger depths.

3. Coarse grids may give erroneous diffraction patterns at the coast with generation of spurious oscillations.

The preceding points suggest that there for a given grid resolution and incident wave may exist an optimal minimum computational depth that is larger than zero. Alternatively, we could apply methods that enable a local refinement and preferably avoid staircase boundaries. Dynamic nesting of a coarse off shore grid with a refined coastal grid meets the first requirement only, unless the coastal grid is curvilinear. Both nesting and practical application of curvilinear grids are, however, hampered

with difficulties. The finite element method meet both requirements, though on the cost of being considerably computationally heavier. Not unlikely, the finite element method may also offer the best opportunities for dynamic nesting in the sense of merging two completely different grids, possibly with different equations implemented, at a common boundary.

The presented work has been carried out under the GITEC (Genesis and Impact of Tsunamis on European Coasts) project that is funded by the European Commission and Norwegian Research Council.

References

[1] Harbitz, C. B. & Pedersen G. 1988 Model theory and analytical solutions for large water waves due to landslides. *University of Oslo, Research Report in Mechanics* **92–4**

[2] Okada, Y. 1985 Surface deformation due to shear and tensile faults in a half-space. *Bull. Seism. Soc. Am.* **75**, 1135-1154

[3] Pedersen, G. 1986 On the effects of irregular boundaries in finite difference models. *Int. J. numer. methods fluids* Vol. **6** 497-505

[4] Pedersen, G., Rygg, O.B. 1987 Numerical solution of the three dimensional Boussinesq equations for dispersive surface waves. *University of Oslo, Research Report in Mechanics No. 1.*

[5] Pedersen G. 1988 Three-dimensional wave patterns generated by moving disturbances at transcritical speeds. *J. Fluid. Mech.* vol. **196** 39-63

[6] Pedersen G. 1988 On the numerical solution of the Boussinesq equations. *University of Oslo, Research Report in Mechanics* **88–14**

[7] Pedersen, G. 1986 On the effects of irregular boundaries in finite difference models. *Int. J. numer. methods fluids* Vol. **6** 497-505

[8] Pedersen G. 1988 Three-dimensional wave patterns generated by moving disturbances at transcritical speeds. *J. Fluid. Mech.* vol. **196** 39-63

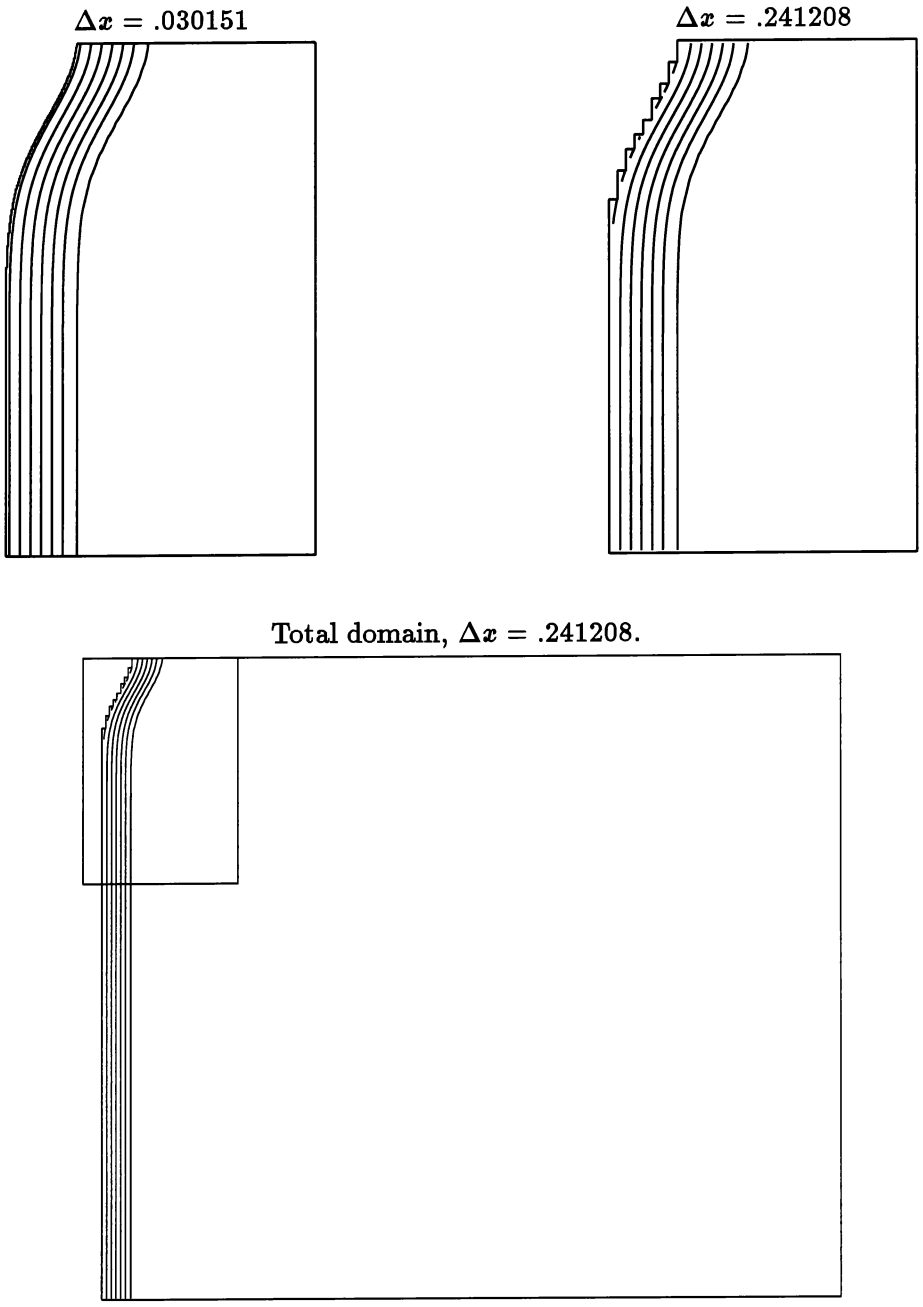

Figure 7: The computational domain depicted with contour increment 0.15. Lower panel displays the total computational domain. Upper panel shows close up on the framed region in lower panel for two different resolutions. The reduced region equals the domain for which the surface elevation is displayed in succeding figures.

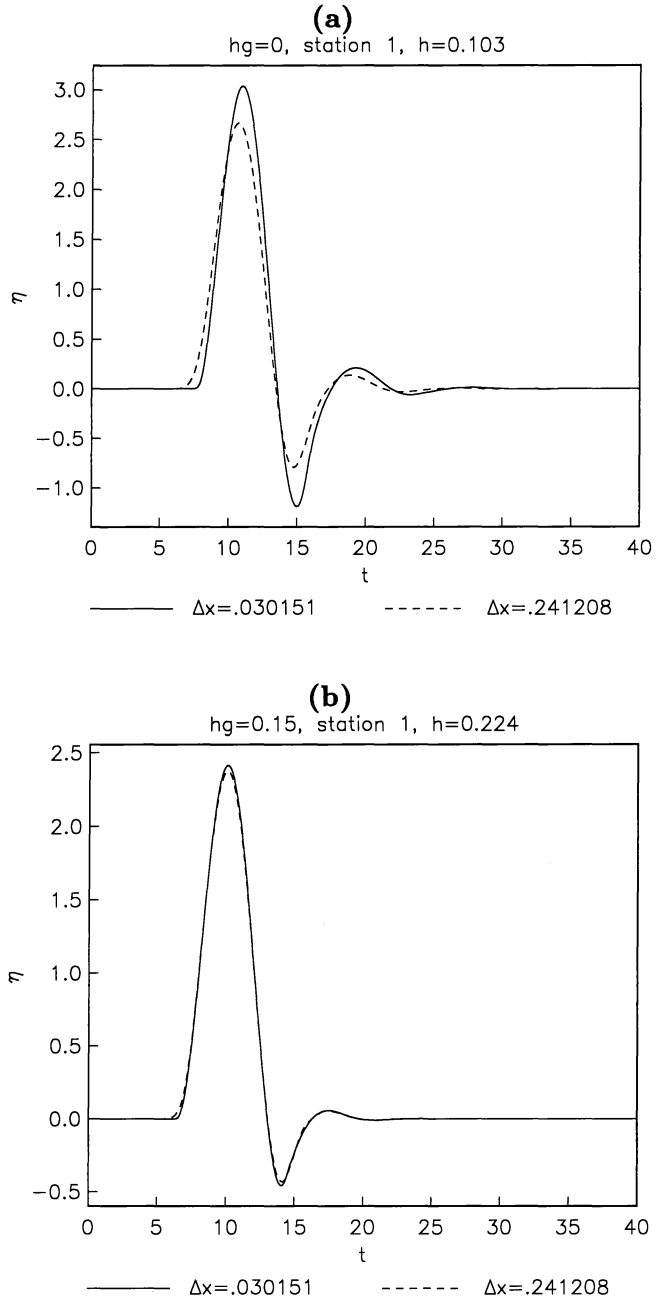

Figure 8: Time series for shallowest point at a straight beach. Upper panel: $h = 0$ as minimum depth, lower panel: $h = 0.15$ as minimum depth.

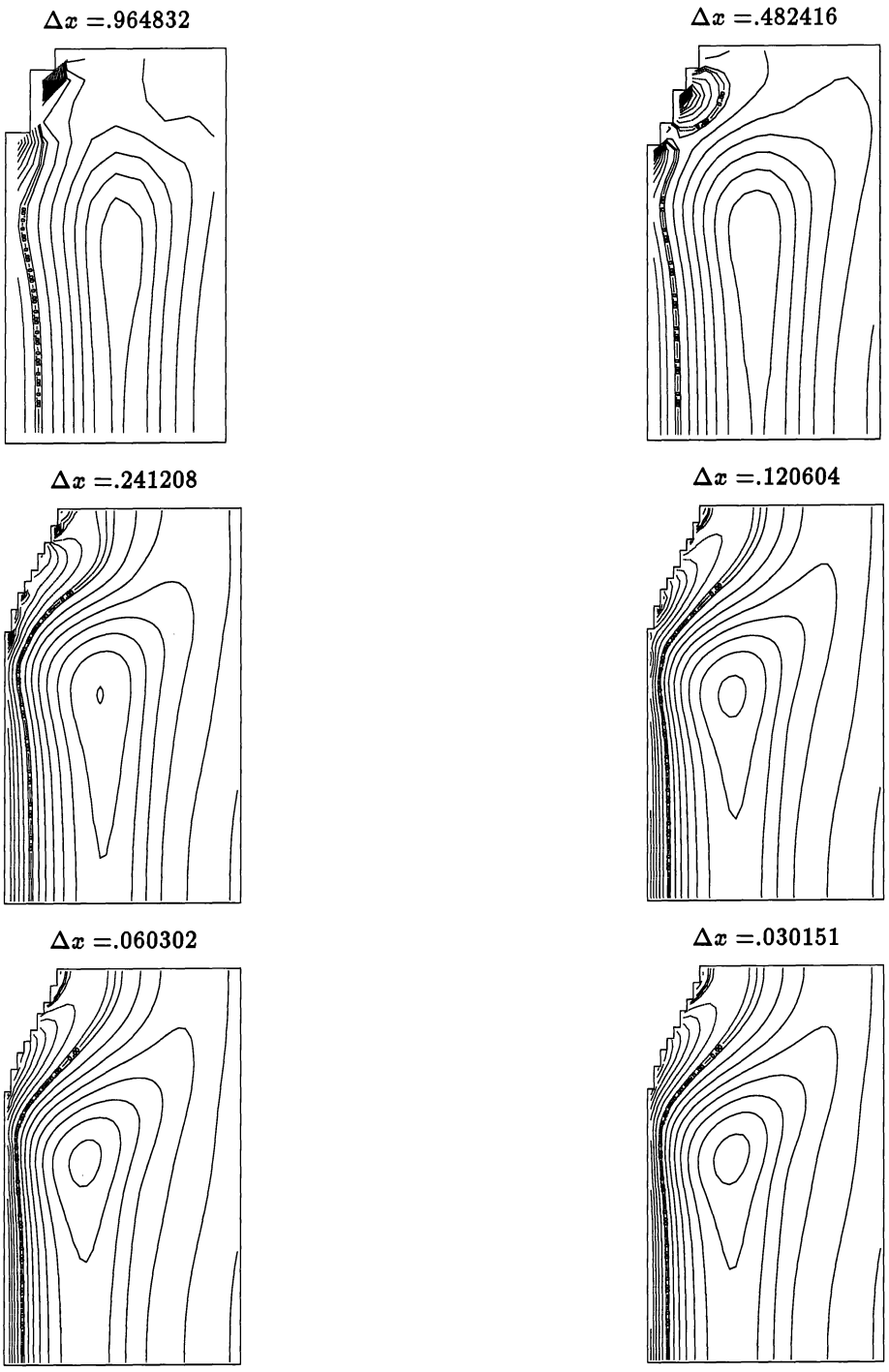

Figure 9: Contour plots, t =15.00. Increment: 0.15.

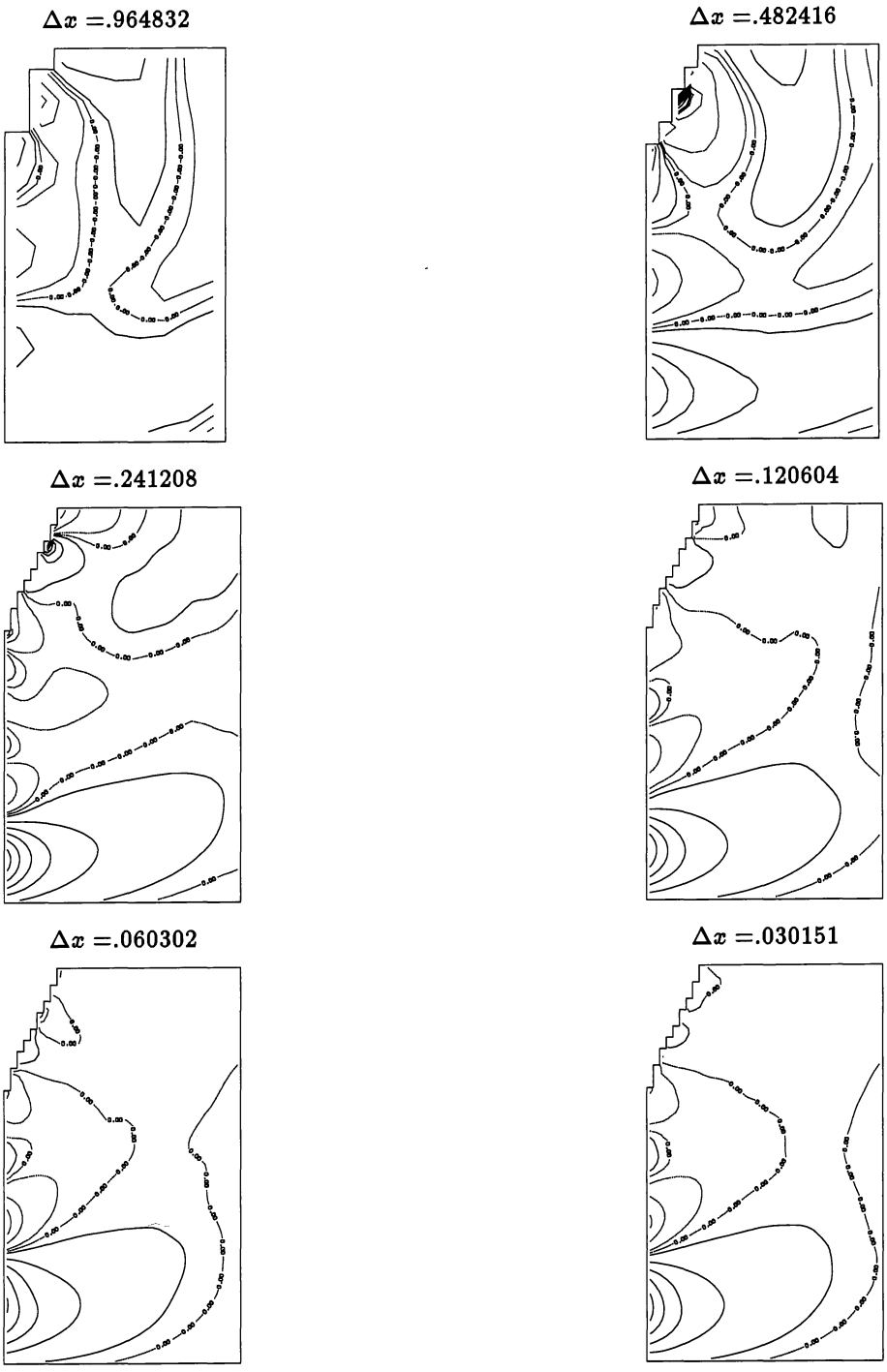

Figure 10: Contour plots, t =33.00. Increment: 0.15.

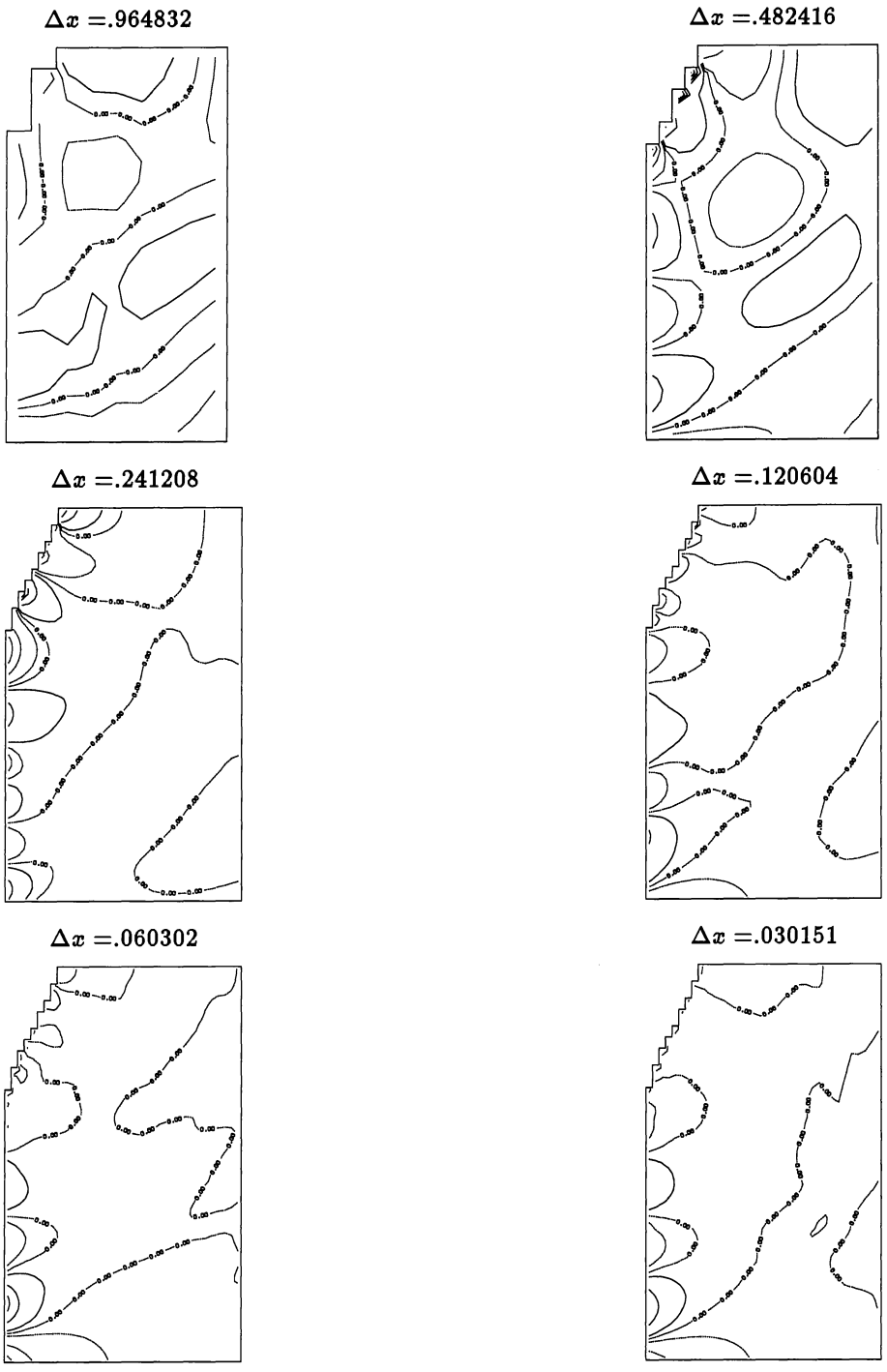

Figure 11: Contour plots, t =42.00. Increment: 0.15.

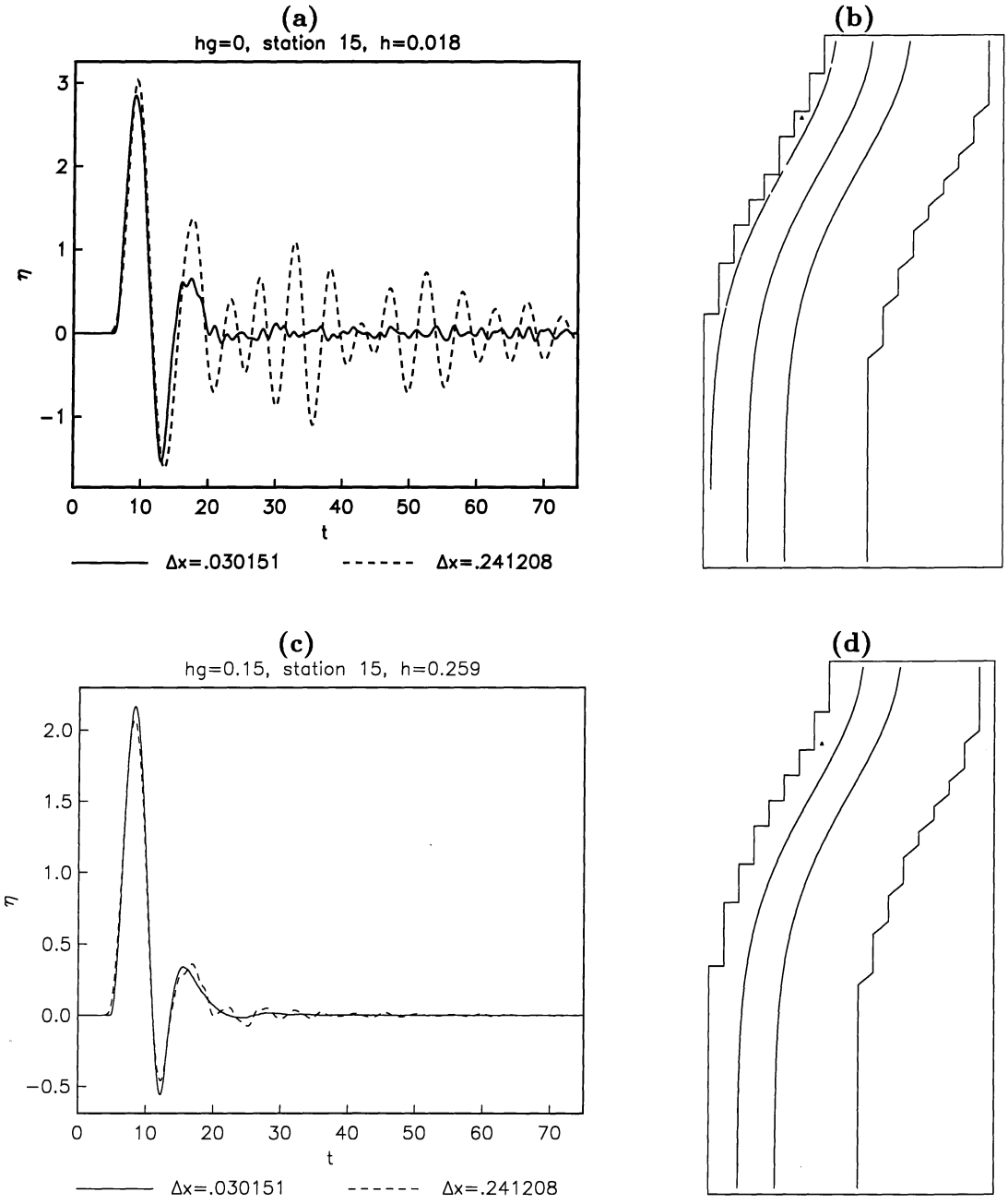

Figure 12: Time series at the peninsula for the shallowest point. Upper panel time series (a) and location of point (b), marked with triangle, for $h = 0$ as minimum computational depth. Corresponding plots for $h = 0.15$ are depicted in lower panel. The depth given above the time series refer to the coarsest grid and the contour plot are depicted with contour increments 0.3.

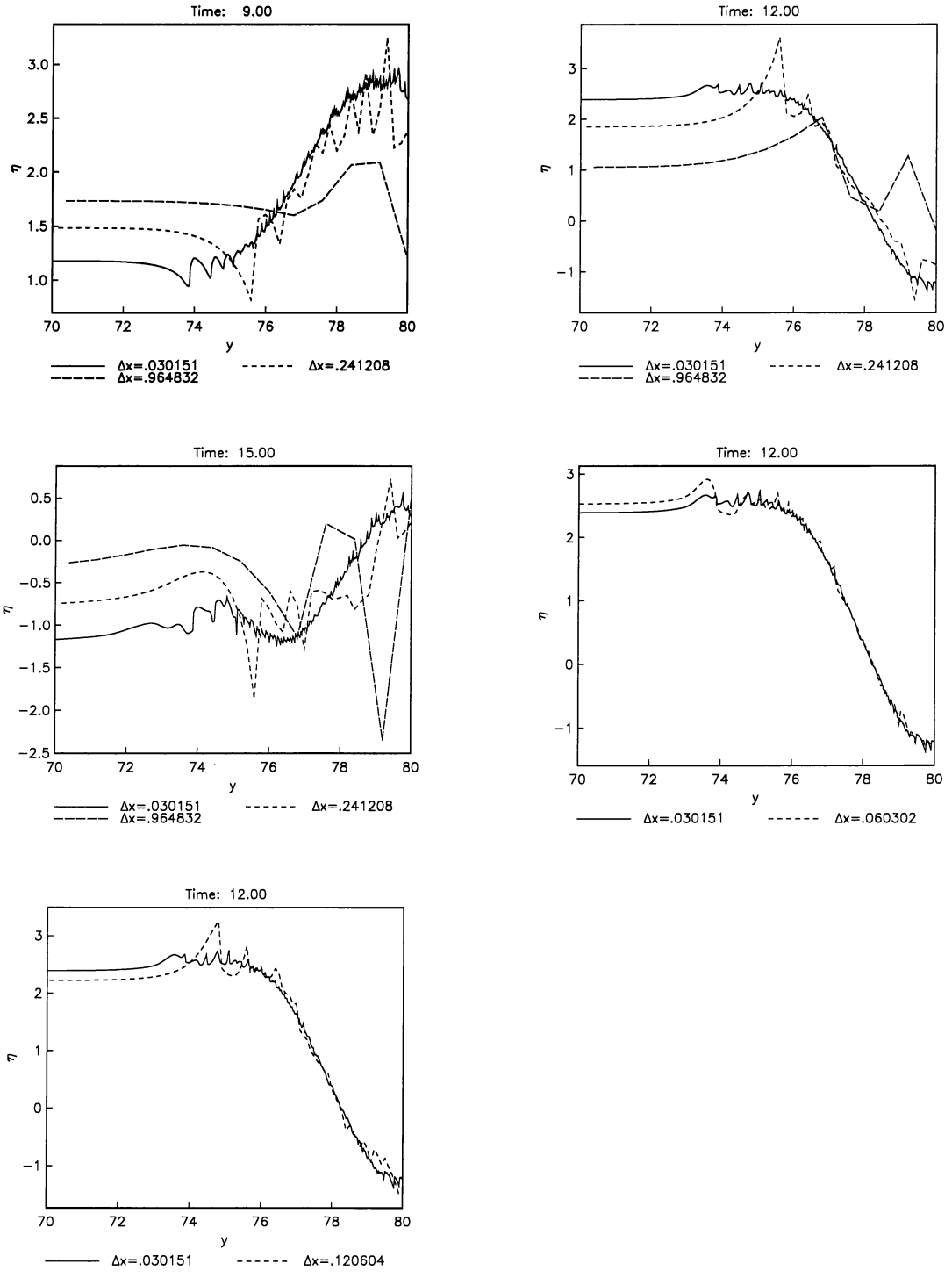

Figure 13: η values adjecant to the shore.

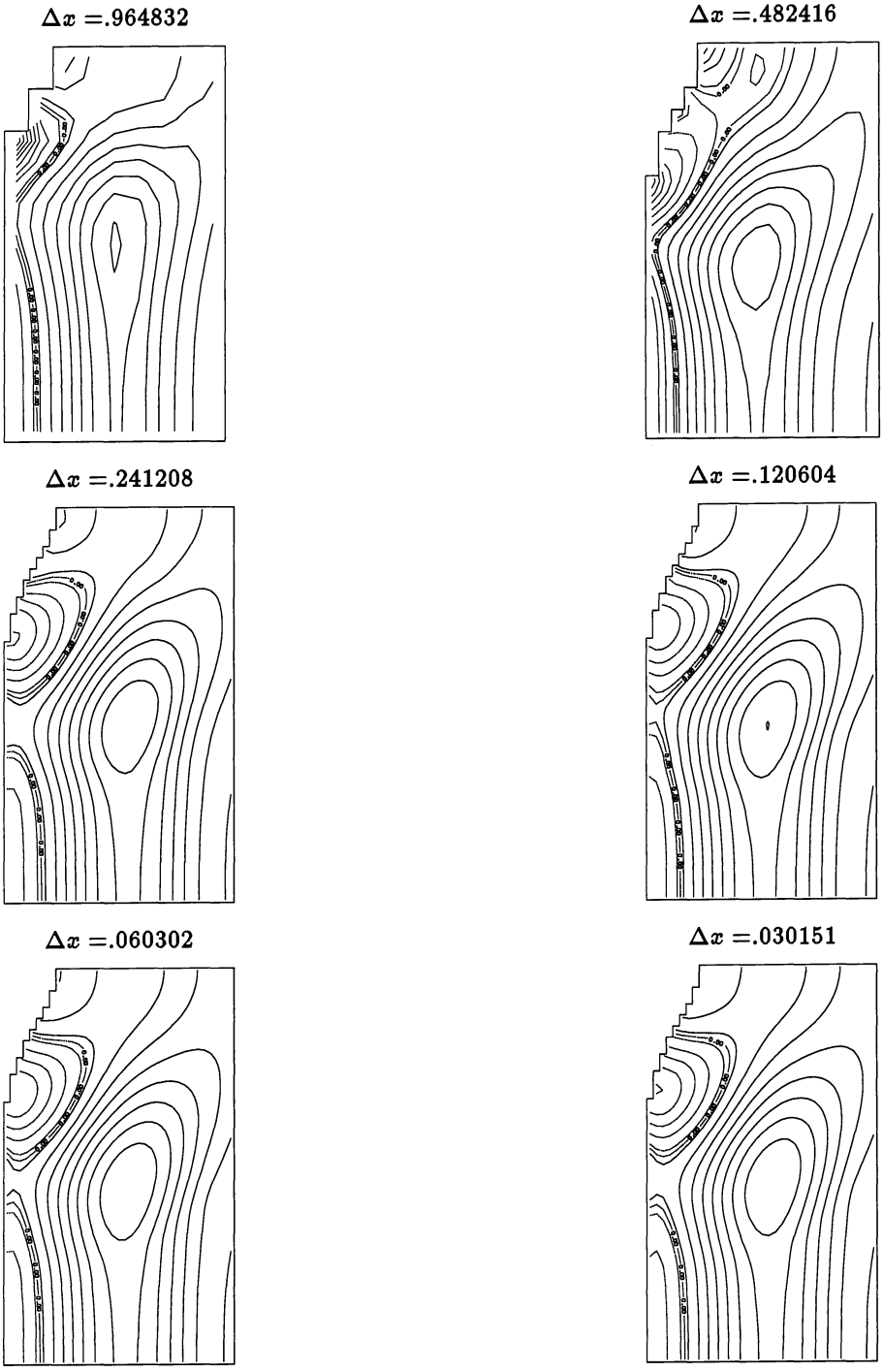

Figure 14: Contour plots at t =15.00 for h =0.15 as minimum computational depth. The contour increment is 0.15.

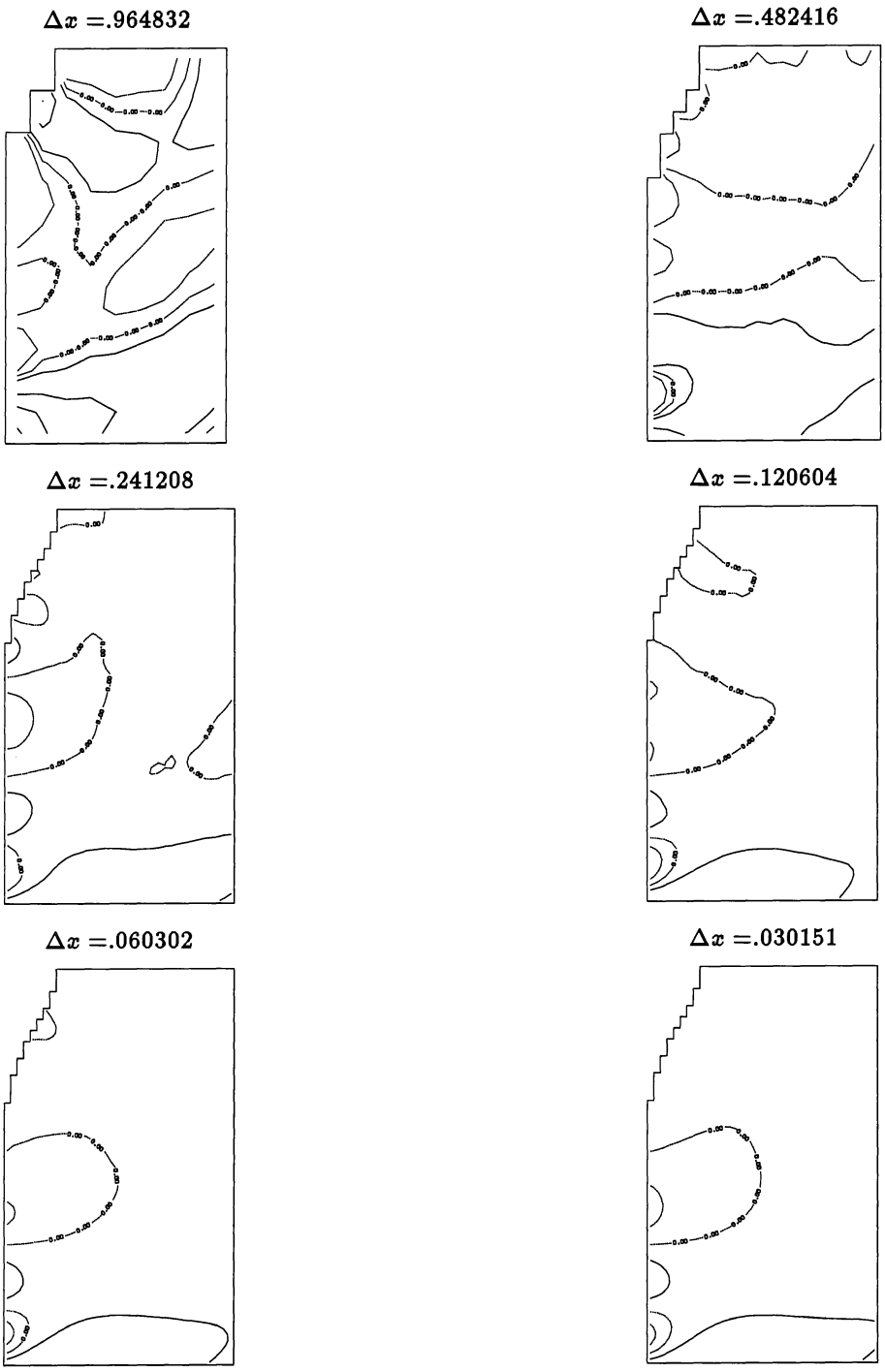

Figure 15: Contour plots at t =33.00 for h =0.15 as minimum computational depth. The contour increment is 0.15.

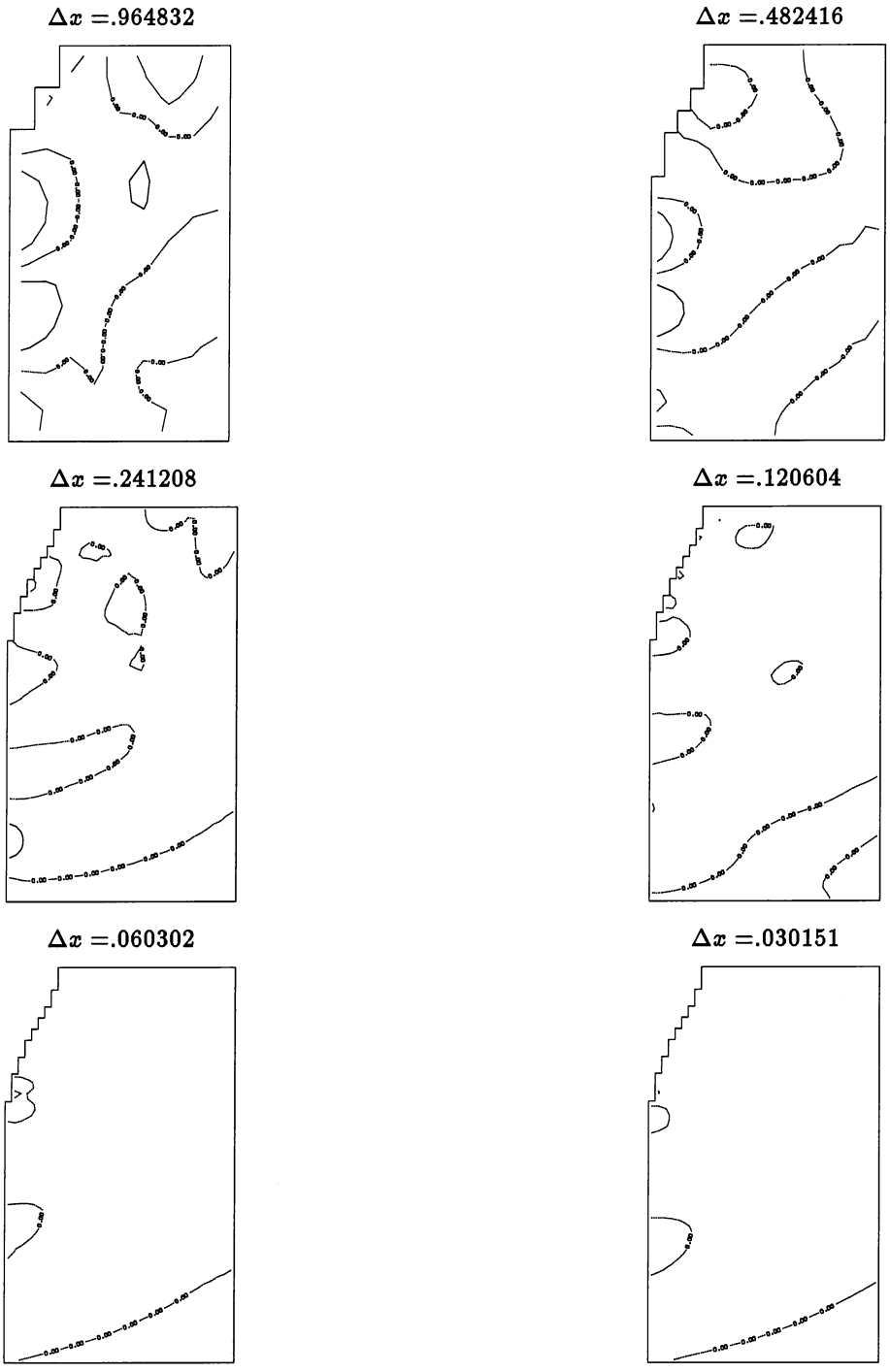

Figure 16: Contour plots at t =42.00 for h =0.15 as minimum computational depth. The contour increment is 0.15.

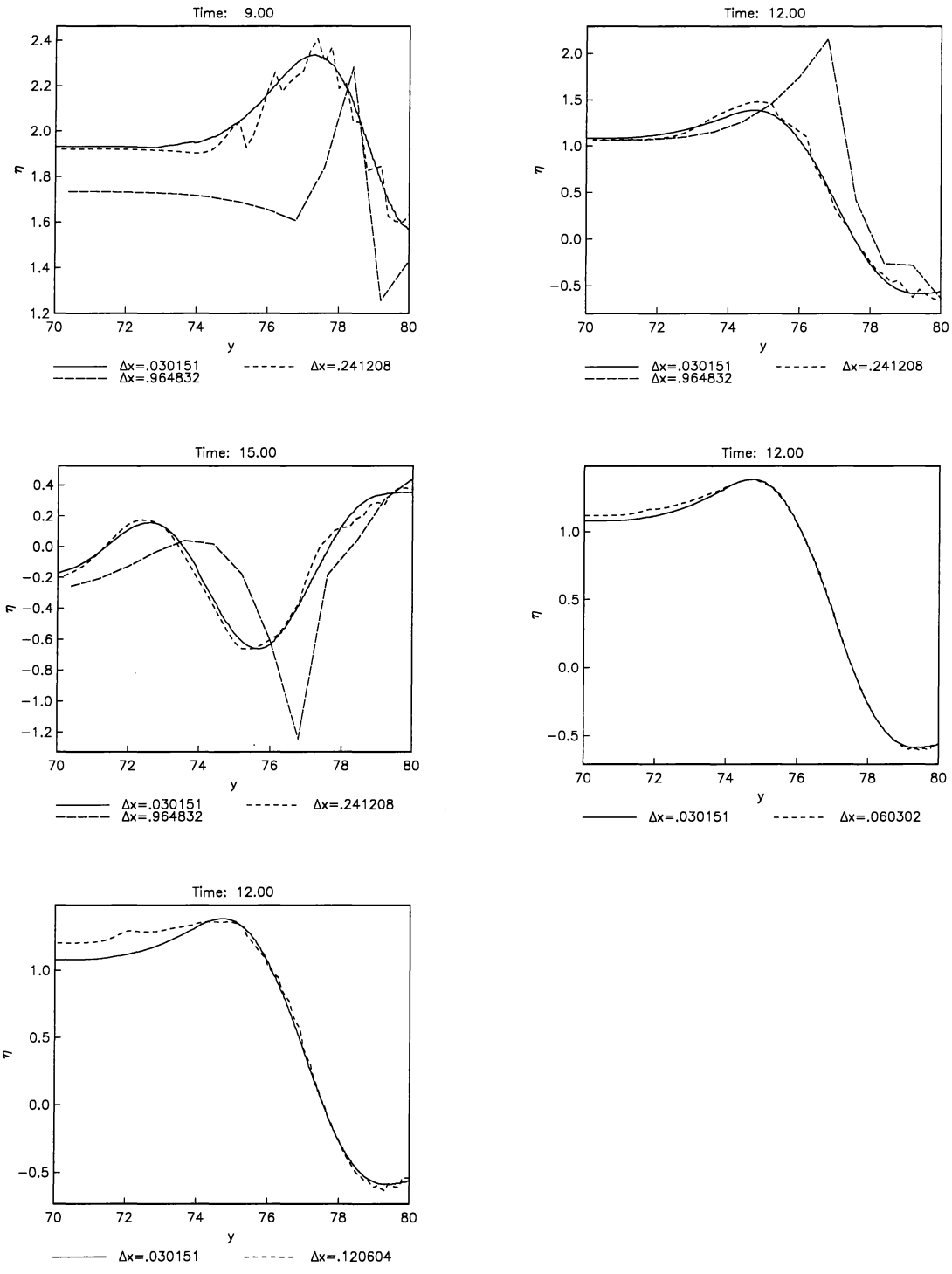

Figure 17: η values adjecant to the shore, for $h = 0.15$ as minimum computational depth.